Geophysical Research Letters

RESEARCH LETTER
10.1029/2019GL083468

Special Section:
Bridging Weather and Climate: Subseasonal-to-Seasonal (S2S) Prediction

A Zonal Migration of Monsoon Moisture Flux Convergence and the Strength of Madden-Julian Oscillation Events

Samson Hagos[1], Chidong Zhang[2], L. Ruby Leung[1], Casey D. Burleyson[1], and Karthik Balaguru[1]

[1]Pacific Northwest National Laboratory, Richland, WA, USA, [2]NOAA Pacific Marine Environmental Laboratory, Seattle, WA, USA

Key Points:
- Moisture convergence centers of the Asian and Australian monsoons migrate zonally across the seasons
- This monsoonal zonal moisture convergence affects the strengths of the zonally propagating Madden-Julian Oscillation (MJO) events
- The Asian and Australian monsoons influence MJO strengths through this moisture convergence migration

Correspondence to:
S. Hagos,
samson.hagos@pnnl.gov

Citation:
Hagos, S., Zhang, C., Leung, L. R., Burleyson, C. D., & Balaguru, K. (2019). A zonal migration of monsoon moisture flux convergence and the strength of Madden-Julian Oscillation events. *Geophysical Research Letters*, *46*, 8554–8562. https://doi.org/10.1029/2019GL083468

Received 24 APR 2019
Accepted 9 JUL 2019
Accepted article online 17 JUL 2019
Published online 31 JUL 2019

Abstract Understanding the variations in the strength of Madden-Julian Oscillation (MJO) events as they propagate across the Indo-Pacific Maritime Continent has been an unmet challenge. Moisture flux convergence estimated directly from precipitation shows a slow eastward migration of zonal moisture flux convergence between the Asian and Australian monsoon convergence centers from summer to winter. Strengths of individual MJO events vary as they propagate across this zonally and seasonally varying monsoonal moisture convergence. MJO events starting in February–April tend to be weak over the eastern Indian Ocean, but they strengthen as they propagate into the moisture convergence region over the western Pacific. During May–July, the moisture convergence pattern is reversed and MJO events weaken as they propagate into the moisture divergence region in the western Pacific. Winter MJO events are most likely to be strong over the Maritime Continent region, particularly when the Australian monsoon is strong.

1. Introduction

The importance of the Madden-Julian Oscillation (MJO; Madden and Julian 1971, 1972) as a potential source of subseasonal-to-seasonal predictability has been well recognized (Vitart et al. 2012; NAS, 2016). While potential predictability of the MJO estimated by dynamical forecast models is up to 4 weeks (Lim et al., 2018; Reichler & Roads, 2005; Waliser et al., 2003), this potential has not yet been fully realized. Neena et al. (2014) showed that the predictive skill limit of the MJO in dynamical models is 5–10 days lower than the potential predictability limit partly because of the lower prediction skills as the MJO crosses the Indo-Pacific Maritime Continent (MC). The problem of this "MC barrier to MJO prediction" is likely a result of limitations in our understanding and, consequently, in model representation of the interaction of MJO convection with the MC. This has inspired several studies to document the seasonality of MJO eastward propagation. These studies have followed two related but parallel paths. Th`e first one involves the use of precipitation tracking methods to characterize the fate of precipitation features associated with MJO events as they cross the MC. Kerns and Chen (2016) used a large-scale precipitation tracking method applied to the Tropical Rainfall Measuring Mission (TRMM) data set and found seasonal and interannual variability in the disruption of MJO propagation by the MC, with MC-crossing events more likely in December and during La Niña years. Another tracking method developed by Ling et al. (2014) and Zhang and Ling (2017), hereafter referred to as ZL17, is based on large-scale equatorial precipitation anomalies (averaged over 10°S–10°N) that move eastward at speeds of 3–7 m/s. Applying this algorithm to daily precipitation from the Tropical Rainfall Measuring mission program (TRMM-342), ZL17 noted a distinction in the spatial distribution of precipitation between propagating and disrupted MJOs. Propagating events rain more over the sea than over land in the MC. Both studies found that nearly half of the MJO events initiated over the Indian Ocean do not propagate across the MC.

In the second approach, the Real-time Multivariate MJO (RMM) index of Wheeler and Hendon (2004) is used to assess the evolution of the overall strength of MJO signals. Following this approach, Burleyson et al. (2018) also found that about half of the MJO events weakened as they crossed the MC while about a quarter were minimally affected and another quarter of the events were strengthened. They also examined the seasonal and interannual variability of disruption and found that MJO events that approach the MC during boreal winter are likely to weaken and weakening MJO events are twice as likely to occur during El Niño years compared to La Niña years.

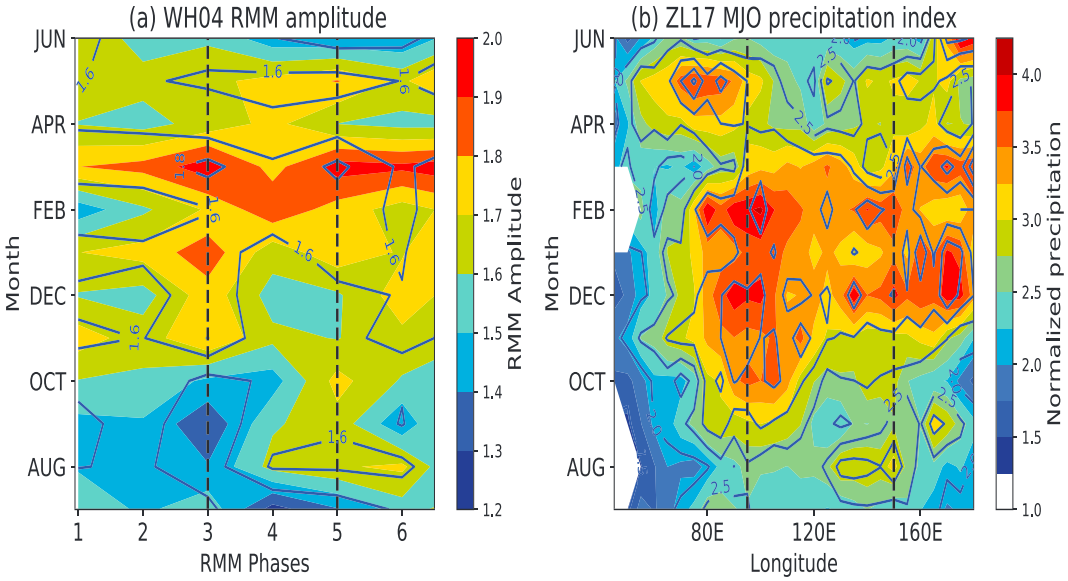

Figure 1. The seasonal cycle of (a) the mean (shaded) and median (contours) RMM amplitudes excluding RMM amplitudes < 1.0, (b) the same for ZL17 normalized MJO precipitation as a function of longitude. The approximate boundaries of the Maritime Continent region are marked by the vertical dashed lines corresponding to RMM phases 3 to 5 and longitudes between 95°E and 150°E. RMM = Real-time Multivariate MJO; MJO = Madden-Julian Oscillation.

Motivated by these results, in this study we examine the large-scale environmental factors in terms of monsoon moisture convergence that may be responsible for the seasonality as well as the role of El Niño-Southern Oscillation (ENSO) in the interannual variability of the strength of MJO events as they cross the MC.

2. The Seasonal Cycle of MJO Strength

We first define MJO strength using the two methods discussed above, the RMM index (Wheeler & Hendon, 2004) and the ZL17 normalized MJO precipitation anomalies obtained by applying the algorithm to National Oceanic and Atmospheric Administration's (NOAA's) Climate Prediction Center Merged Analysis of Precipitation (CMAP) pentad precipitation. Figure 1 shows the seasonal cycle of MJO strength as represented by the mean of RMM and ZL17 amplitudes for each month over all the years. Only amplitudes >1.0 are included in the seasonal cycles. Despite significant differences in detail, there are similarities between the MJO strength represented by the two methods. First, MJO events are well known to be strong during boreal fall and winter and generally weak during boreal summer (Zhang & Dong, 2004), which is apparent in both panels. Second, MJO events tend to be strongest over the western and eastern boundaries of the MC region, which are approximated by the dashed lines at 95°E and 150°E (phases 3 and 5 in the RMM index). Seasonally, the peak over the eastern boundary of the MC region occurs later than that over the western boundary. Third, the peaks of MJO events over the western and eastern edges of the MC region extend into the interior of the MC during winter, suggesting a higher likelihood of MJO events propagating across the MC during boreal winter. For brevity, the region west of the 95°E and east of 150°E will be referred to as eastern Indian Ocean and western Pacific, respectively, while the area in between will be simply referred to as the MC region. In order to understand the seasonality of MJO events, we examine their sources of moisture and how they are influenced by seasonally varying large-scale processes.

3. Method

The steady state form of the vertically integrated moisture budget equation is

$$-\nabla\cdot\frac{1}{g}\int_{ps}^{pt}(q\boldsymbol{v})dp\simeq P-E \tag{1}$$

where P is precipitation, E is evaporation, q is water vapor mixing ratio, and v is horizontal wind. One can define a moisture flux potential Φ as

$$-\nabla^2\Phi \simeq P-E \tag{2}$$

and a moisture flux vector field

$$\boldsymbol{v}_q = \nabla\cdot\Phi \tag{3}$$

Physically, unlike the moisture convergence itself, moisture flux potential is nonlocal, and its gradient (equation (3)) represents the direction and magnitude of net divergent moisture transport. Specifically, the local maximum and minimum of Φ represent a moisture source and a sink, respectively. Given the total vertically integrated moisture convergence (or, alternatively, $P-E$), the Poisson equation (equation (2)) can be solved for the moisture flux potential and the moisture flux vectors. The main advantage of this approach is that the moisture transport can be directly estimated from the observed precipitation and evaporation. Focusing on the moisture transport associated directly with precipitation, we ignore the contribution of evaporation and calculate the moisture transport associated only with precipitation. In this case the contributions of the zonal and meridional components of moisture convergence to local precipitation are

$$P_x = -\frac{\partial^2\Phi}{\partial x^2} \tag{4}$$

and

$$P_y = -\frac{\partial^2\Phi}{\partial y^2} \tag{5}$$

The moisture flux potential and moisture flux are calculated by solving equation (2) using 30 years (1983–2012) of daily precipitation from the Precipitation Estimation from Remotely Sensed Information using Artificial Neural Networks (PERSIANN; Ashouri et al. 2018) data set at 0.25° grid spacing.

The seasonal and interannual behaviors of the solution to equation (2) based on the PERSIANN daily precipitation is shown in Figure 2. The top panels show the 30-year means of zonal (shadings) and meridional (contours) moisture flux convergence and moisture flux vectors for January and July. The bottom panels show their differences between El Niño and La Niña years for the 2 months. El Niño and La Niña years are defined by the NOAA Climate Prediction Center's Ocean Niño Index (3-monthly running mean $\pm$ 0.5 °C sea surface temperature anomalies over the Niño 3.4 region). On a seasonal time scale, the divergent circulation representing the moisture transport associated with the monsoons is obvious. To the first order, moisture convergence is dominated by its meridional component, with meridional moisture convergence occurring broadly south of the equator in the tropics in January during the Australian monsoon season, which switches to meridional moisture divergence in July during the Asian monsoon season. The centers of the meridional moisture convergence in both seasons are collocated with the pathways of MJO events propagating through the MC as identified by ZL17.

There is also a significant zonal component (shadings) associated with the convergence centers of the Asian and Australian monsoons at different longitudes. In January, anomalous moisture divergence is present over the eastern Indian Ocean and western Pacific, while moisture convergence occurs over the MC region. In July the pattern is reversed with convergence over the eastern Indian Ocean and western Pacific and the two oceanic regions and with weak divergence over the MC region. These patterns lead us to hypothesize that the seasonality of MJO strength, particularly the extension of the peaks over the western and eastern edges of the MC region into its interior in winter, might be related to the seasonally varying moisture convergence pattern. This hypothesis is examined in the next section. On the interannual time scale (Figures 2c and 2d), moisture is transported from the MC to the central tropical Pacific in both January and July during El Niño years relative to La Niña years. In July the anomalous moisture flux associated with El Niño is oriented northwestward from the equator.

4. Seasonal Cycle of Moisture Supply for MJO Precipitation

Taking advantage of estimated moisture flux from precipitation, we examine the seasonal cycles of the zonal and meridional moisture convergence associated with monsoon precipitation near the equator (averaged between 15°S and 15°N). Both precipitation and the zonal component of moisture flux convergence start

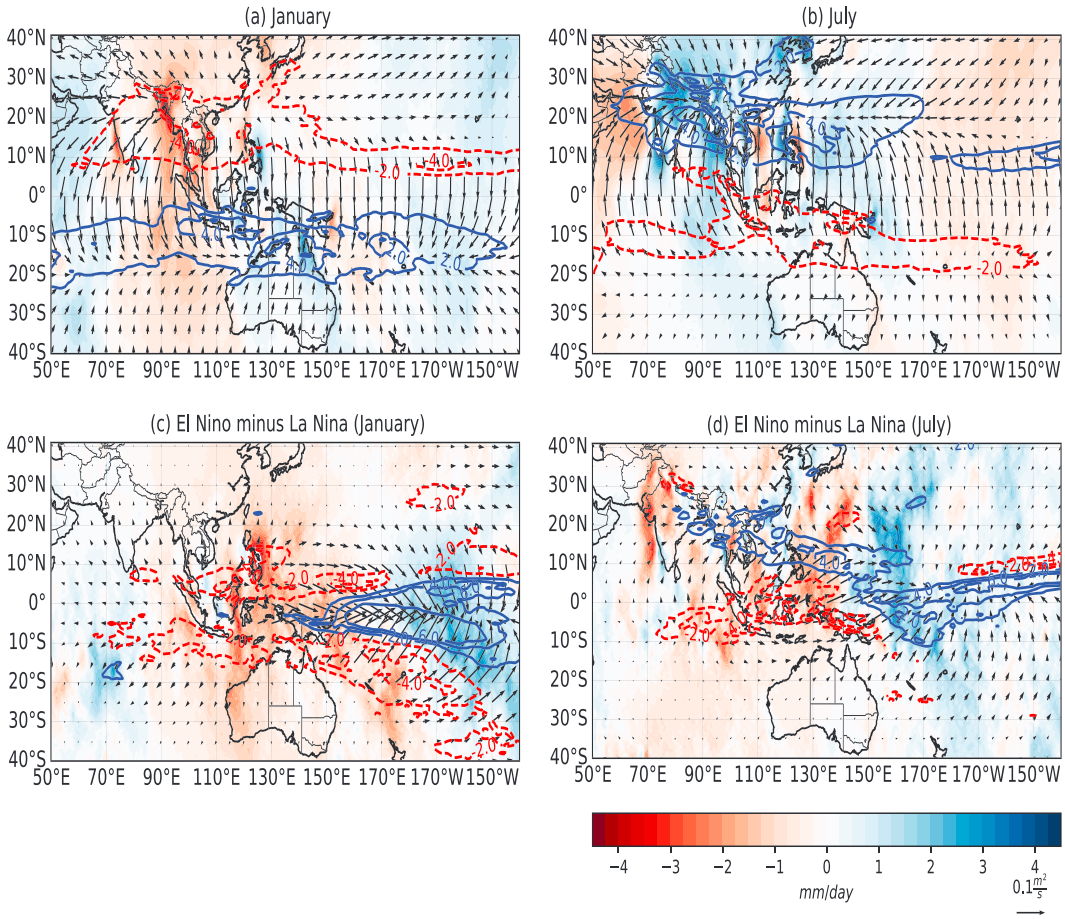

Figure 2. Climatological zonal (shadings) and meridional (contours) moisture flux convergence and moisture flux (arrows) for (a) January and (b) July. The difference between El Niño and La Niña years are shown in (c) for January and (d) July.

over the central Indian Ocean (~80°E) during boreal summer and migrate eastward until reaching their farthest points in April (Figure 3a). Their divergent phases start migrating eastward in November so a zonal contrast in convergence is maintained. There is also a zonal migration of the meridional component (Figure 3b), which is most prominent between October and March when the north-south movement of the monsoon convergence arrives at the equator as it propagates to the Australian monsoon region. The seasonal migration of both the zonal and meridional moisture convergence is broadly consistent with Figure 2, but the seasonality is more obvious in the Hovmöller diagrams. Both zonal and meridional components of the moisture flux convergence related to the MJO (conditioned by RMM amplitudes greater than 1.0) show seasonally and zonally migrating signals (Figures 3c and 3d) as seen in the monsoon (Figures 3a and 3b). The zonal variability in the seasonal cycle that is most relevant to the lifecycle of the individual MJO events is more prominent in the zonal component. Specifically, from July to October, strong MJO signals migrate from favorable (positive) zonal moisture convergence over eastern Indian Ocean provided by the monsoon to unfavorable (moisture divergence) over the MC region. From November to April they propagate from unfavorable to favorable environments. Meanwhile, the meridional component of moisture flux convergence is favorable between October and March and shows less zonal variability. The seasonal migration of zonal moisture convergence of the monsoon lends support to its influence on MJO events, particularly their strengthening in the MC region during winter and the later MJO peaks in the eastern boundary of the MC compared to the western boundary (Figure 1). In contrast, for the non-MJO component (conditioned by RMM amplitude of less than 1.0), the seasonal zonally migrating moisture flux convergence is much weaker (Figures 3e and 3f). This suggests that the influence of the monsoon environment on the MJO is unique, perhaps more germane to MJO dynamics than to other convective systems.

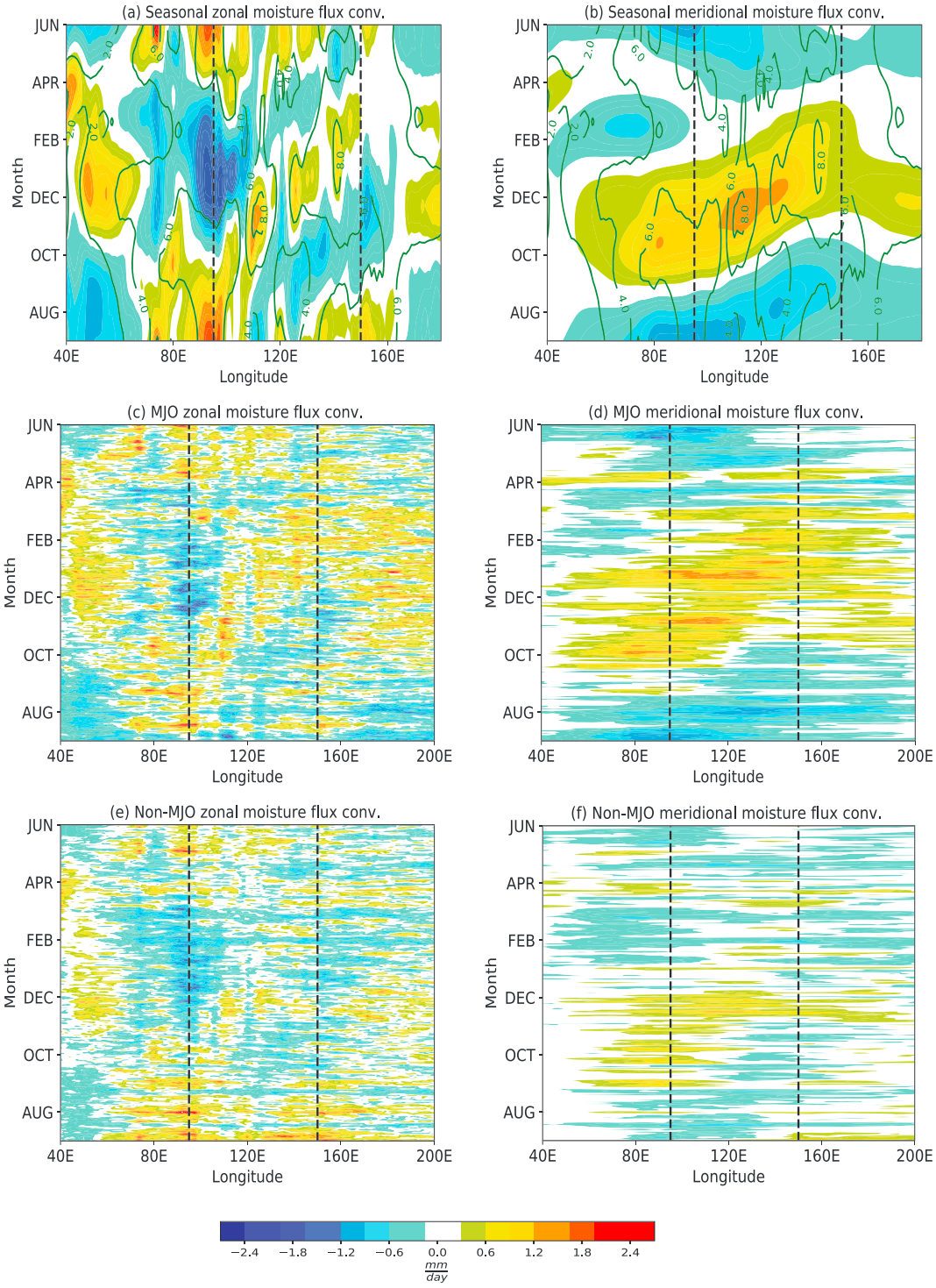

Figure 3. Seasonal cycles of the total (a) zonal and (b) meridonal components of moisture flux convergence (shadings) overlaid on precipitation (contours); (c and d) the same but only for when the RMM amplitude is greater than 1.0; (e and f) similar to (c) and (d) but for the RMM amplitude less than 1.0. All are averaged between 15°S and 15°N. The dashed lines mark the approximate boundary of the Maritime Continent region.

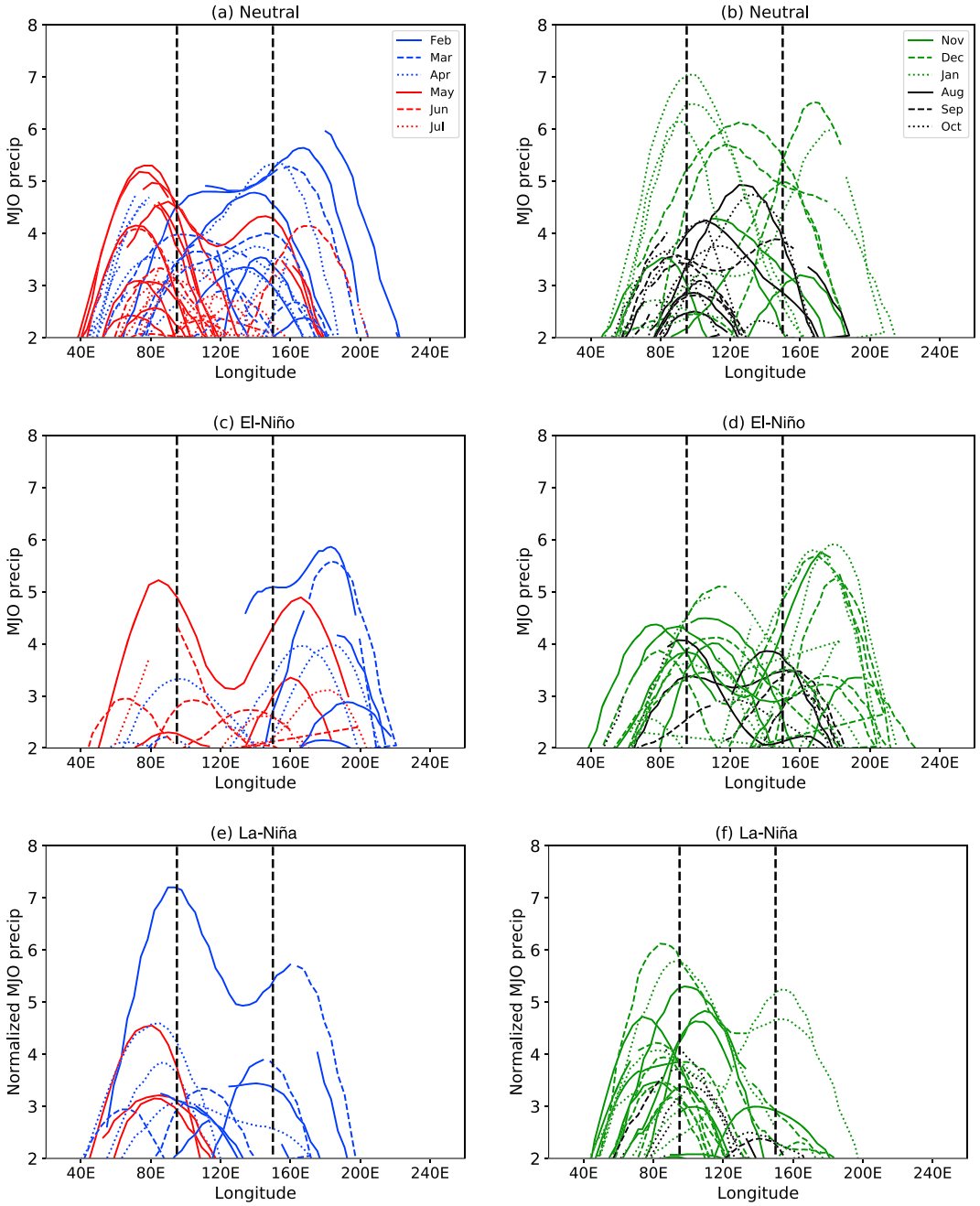

Figure 4. Evolution of the ZL17 normalized precipitation index for individual Madden-Julian Oscillation (MJO) events during (top) neutral, (middle) El Niño, and (bottom) La Niña years. The vertical dashed lines mark the approximate boundaries of the Maritime Continent region.

Before we examine the behavior of individual MJO events, some discussion of our result in the context of existing literature is warranted. Given three-dimensional wind and moisture data, the "MJO" moisture flux convergence discussed above can be partitioned into advective and wind convergence components, which can further be partitioned into advection of background moisture by the MJO, advection of MJO moisture by the background wind, and so on. In fact, such analysis has been performed by a large number of studies using global reanalyses, model simulations, or data from limited area array of soundings. In general, those studies aimed at understanding the propagation mechanism of the MJO, and they highlight two primary mechanisms for MJO propagation: (1) advection of background moisture by MJO winds (Adames, 2017; Kim et al., 2014; Maloney, 2009; Pritchard & Bretherton, 2014; Sobel & Maloney, 2013) and (2) a

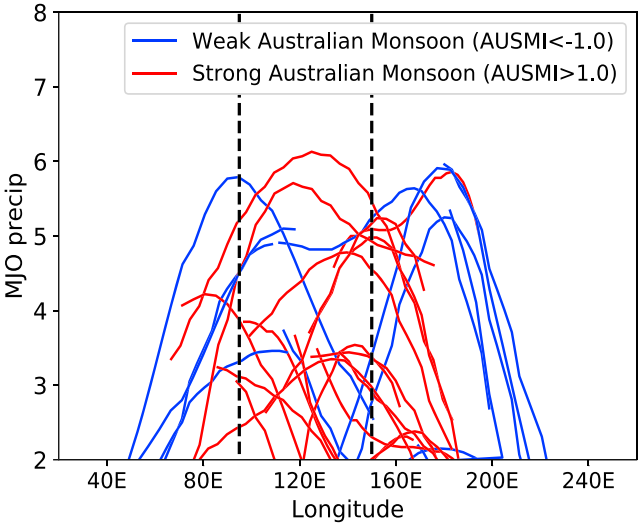

Figure 5. Strength of December, January, and February Madden-Julian Oscillation (MJO) events represented by the ZL17 normalized precipitation during weak and strong Australian monsoon months represented by the Australian monsoon index (AUSMI) of Kajikawa et al. (2010).

combination of cloud radiative feedbacks and upper-level circulations (Bony and Emanuel 2005, Powell & Houze, 2015, Kim et al., 2016). Our method of calculating moisture flux convergence from only the observed precipitation cannot separate the contribution of background wind, background convergence, or background moisture. Therefore, this study is agnostic to which mechanism is primarily responsible for the propagation of the MJO. Regardless of how the background state influences the MJO propagation (wind, moisture, or some combination thereof), its seasonal zonal movement influences the propagation behavior of individual MJO events, as we will further demonstrate below.

The above results from the moisture budget analysis can be verified by directly analyzing the evolution of individual MJO events observed during different months as they propagate eastward using the ZL17 tracks discussed above. Figure 4 shows the strength of each tracked MJO event measured by its precipitation along the equator (10°S–10°N) under neutral, El Niño, and La Niña conditions separately for February to July (left panels) and August to January (right panels). Despite large variability among the MJO events, the seasonality in their strength is consistent with the results of the moisture budget analysis. Out of 73 MJO events observed during the months of February, March, and April (blue), only 16 have their peak strength occurring over the eastern Indian Ocean. On the other hand, for May, June, and July (red), 30 out of 59 events peak over the eastern Indian Ocean. Many events in November, December, and January (green) are strong, and their peak amplitude is more likely to be over the MC region or over the Pacific Ocean. Only 22 out 87 events have their peak over the eastern Indian Ocean. Events in August, September, and October (black) are relatively weak as a reflection of the meridional movement of the monsoon precipitation (Figures 3b and 3d). Similar behavior is observed during El Niño and La Niña conditions except MJO events over the Indian Ocean are stronger during La Niña and are weaker during El Niño and the reverse is true over the central Pacific. This is consistent with the background zonal moisture convergence anomalies in the two ENSO phases (Figures 2c and 2d).

Finally, the relationship between the zonal structures of MJO strength with the monsoon is examined using an index for Australian monsoon developed by Kajikawa et al. (2010). The index is the normalized monthly mean 850-hPa zonal wind averaged over (110–130°E, 15–5°S) for December, January, and February. Figure 5 shows the ZL17 normalized precipitation index for MJO events during weak and strong Australian monsoon months. With a stronger (weaker) Australian monsoon, the zonal moisture convergence in the MC region during winter will be stronger (weaker; Figures 2a and 3a). Consistent with the influence of the monsoon on zonal moisture convergence, MJO events tend to be strongest over the MC region during strong monsoon months, with seven out of nine events having their peak over the MC. On the contrary, during weak monsoon years MJO events are stronger east and west of the MC region.

5. Conclusion

To understand factors controlling the variability in the strength of MJO events during their lifetime including their strengthening and weakening after they form as well as their propagation across the Indo-Pacific MC region, we examined their sources of moisture by directly calculating the moisture flux potential, the moisture flux, and the zonal and meridional components of moisture flux convergence directly from observed precipitation. Using two metrics for MJO strength, the RMM index and the tracked and normalized MJO precipitation anomalies of Zhang and Ling (2017), we have shown that the strength of MJO precipitation is regulated by seasonal anomalies in zonal moisture flux convergence of the monsoons that starts in the central equatorial Indian Ocean during the Asian summer monsoon season, migrates eastward, and ends over the eastern boundary of the MC region at the end of the Australian monsoon season (Fig. 3a). Depending on the season, MJO events may encounter favorable environment associated with moisture convergence at different longitudes. In February, March, and April, MJO events tend to start weak in the divergence regime over the eastern Indian Ocean and strengthen as they propagate into the convergence

regime over the western Pacific (Figure 4). In contrast, in May, June, and July, MJO events are most likely to weaken as they propagate from the regime of anomalous moisture convergence to that of divergence. In a similar manner, during El Niño years, MJO events are likely to be weakened as they propagate across the anomalous divergence over the western Indian Ocean and MC region and strengthened over the central Pacific convergence (Figures 4d and 4f). While MJO events are usually strong at either the eastern Indian Ocean or the western Pacific, peak MJO strength is also observed over the MC region, particularly during strong Australian monsoon months (Figure 5) that strengthen the moisture convergence over the MC region.

The seasonality and interannual variability of MJO events observed in this study are in general agreement with those discussed by Kerns and Chen (2016), who used a different tracking method. They also found that precipitation signals in December are more common than in other months and during La Niña years. However, we found more and stronger MJO events over the central Pacific during El Niño years than during La Niña years (Figure 4c). When it comes to processes, the results from this study are in agreement with the recent study by DeMott et al. (2018) that also highlighted the role of precursor moisture conditions to the immediate east of MJO convection centers influencing their strengthening and weakening and the role of ENSO in setting the zonal structure of the precursor moisture conditions. This study does not address mechanisms of how moisture convergence control MJO propagation or weakening and strengthening of the MJO arising from other processes such as land surface conditions over the MC or feedback from air-sea interactions over the equatorial eastern Indian and western Pacific oceans (Benedict and Randall 2011), during the same season and under similar monsoon or ENSO conditions. This study suggests, however, that analyzing MJO behaviors relative to the zonally varying moisture supply controlled by the monsoons, ENSO, and possibly other phenomena in addition to geographical locations may potentially help to identify other mechanisms for the observed MJO variability and help to identify sources of variations in MJO predictability.

Acknowledgments
This work is supported by the National Oceanic and Atmospheric Administration (NOAA) Oceanic and Atmospheric Research, Climate Program Office (CPO), under NOAA grant number NA17OAR4310263, as well as the U.S. Department of Energy Office of Science Biological and Environmental Research as part of the Atmospheric Systems Research Program and Global and Regional Modeling Program. Computing resources are provided by the National Energy Research Scientific Computing Center (NERSC). Pacific Northwest National Laboratory is operated by Battelle for the U.S. Department of Energy under contract DE-AC05-76RLO1830. C. Z. is supported by Pacific Marine Environmental Laboratory contribution 4850. Daily time series of the RMM index are available at http://www.bom.gov.au/climate/mjo/graphics/rmm.74toRealtime.txt, accessed on 13 January 2016. The precipitation and ENSO index data sets are available at https://www.esrl.noaa.gov/psd/data/index.html.The Australian monsoon index is obtained from http://apdrc.soest.hawaii.edu/projects/monsoon/definition.html#ausm.

References

Adames, Á. F. (2017). Precipitation budget of the Madden-Julian Oscillation. *Journal of the Atmospheric Sciences*, *74*(6), 1799–1817. https://doi.org/10.1175/JAS-D-16-0242.1

Burleyson, C. D., Hagos, S. M., Feng, Z., Kerns, B. W. J., & Kim, D. (2018). Large-scale environmental characteristics of MJOs that strengthen and weaken over the Maritime Continent. *Journal of Climate*, *31*(14), 5731–5748. https://doi.org/10.1175/JCLI-D-17-0576.1

DeMott, C. A., Wolding, B. O., Maloney, E. D., & Randall, D. A. (2018). Atmospheric mechanisms for MJO decay over the Maritime Continent. *Journal of Geophysical Research: Atmospheres*, *123*(10), 5188–5204. https://doi.org/10.1029/2017JD026979

Kajikawa, Y., Wang, B., & Yang, J. (2010). A multi-time scale Australian monsoon index. *International Journal of Climatology*, *30*(8), 1114–1120. https://doi.org/10.1002/joc.1955

Kerns, B. W., & Chen, S. S. (2016). Large-scale precipitation tracking and the MJO over the Maritime Continent and Indo-Pacific warm pool. *Journal of Geophysical Research: Atmospheres*, *121*, 8755–8776. https://doi.org/10.1002/2015JD024661

Kim, D., Kug, J.-S., & Sobel, A. H. (2014). Propagating versus non-propagating Madden-Julian oscillation events. *Journal of Climate*, *27*(1), 111–125. https://doi.org/10.1175/JCLI-D-13-00084.1

Kim, H. M., Kim, D., Vitart, F., Toma, V. E., Kug, J. S., & Webster, P. J. (2016). MJO propagation across the Maritime Continent in the ECMWF ensemble prediction system. *Journal of Climate*, *29*(11), 3973–3988. https://doi.org/10.1175/JCLI-D-15-0862.1

Lim, Y., Son, S., & Kim, D. (2018). MJO prediction skill of the subseasonal-to-seasonal prediction models. *Journal of Climate*, *31*(10), 4075–4094. https://doi.org/10.1175/JCLI-D-17-0545.1

Maloney, E. D. (2009). The moist static energy budget of a composite tropical intraseasonal oscillation in a climate model. *Journal of Climate*, *22*(3), 711–729. https://doi.org/10.1175/2008JCLI2542.1

National Academies of Sciences, Engineering, and Medicine (2016). *Next generation Earth system prediction: Strategies for subseasonal to seasonal forecasts*. Washington, DC: The National Academies Press.

Neena JM, Lee JY, Waliser D, Wang B, Jiang X. 2014. Predictability of the Madden–Julian Oscillation in the Intraseasonal Variability Hindcast Experiment (ISVHE). *Journal of Climate 27*: 4531–4543. https://doi.org/10.1175/ JCLI-D-13-00624.1, 12, DOI: https://doi.org/10.1175/JCLI-D-13-00624.1

Powell, S. W., & Houze, R. A. Jr. (2015). Effect of dry large-scale vertical motions on initial MJO convective onset. *Journal of Geophysical Research: Atmospheres*, *120*, 4783–4805. https://doi.org/10.1002/2014JD022961

Pritchard, M. S., & Bretherton, C. S. (2014). Causal evidence that rotational moisture advection is critical to the superparameterized Madden–Julian Oscillation. *Journal of the Atmospheric Sciences*, *71*(2), 800–815. https://doi.org/10.1175/JAS-D-13-0119.1

Reichler, T., & Roads, J. O. (2005). Long-range predictability in the tropics. Part II: 30–60-day variability. *Journal of Climate*, *18*(5), 634–650. https://doi.org/10.1175/JCLI-3295.1

Sobel, A. H., & Maloney, E. (2013). Moisture modes and the eastward propagation of the MJO. J. Atmos. Sci., 70, 187–192, Vitart F, Robertson DA. 2012. Sub-seasonal to seasonal prediction project: Bridging the gap between weather and climate. *WMO Bulletin*, *61*, 23–28.

Waliser, D. E., Lau, K. M., Stern, W., & Jones, C. (2003). Potential predictability of the Madden–Julian Oscillation. *Bull. Amer. Meteor. Soc*, *84*(1), 33–50. https://doi.org/10.1175/BAMS-84-1-33

Wheeler, M. C., & Hendon, H. H. (2004). An all-season real-time multivariate MJO index: Development of an index for monitoring and prediction. *Monthly Weather Review*, *132*(8), 1917–1932. https://doi.org/10.1175/1520-0493(2004)132<1917:AARMMI>2.0.CO;2

Zhang, C., & Dong, M. (2004). Seasonality in the Madden–Julian Oscillation. *Journal of Climate*, *17*(16), 3169–3180. https://doi.org/10.1175/1520-0442(2004)017<3169:SITMO>2.0.CO;2

Zhang, C., & Ling, J. (2017). Barrier effect of the Indo-Pacific Maritime Continent on the MJO: Perspectives from tracking MJO precipitation. *Journal of Climate*, *30*(9), 3439–3459. https://doi.org/10.1175/JCLI-D-16-0614.1